Enhanced CO_2 Hydrogenation to Methanol over CuZn Nanoalloy in Ga Modified Cu/ZnO Catalysts

Molly Meng-Jung Li[1], Ziyan Zeng[2], Fenglin Liao[1], Xinlin Hong[2], Shik Chi Edman Tsang[1*]

[1] *Wolfson Catalysis Centre, Department of Chemistry, University of Oxford, Oxford, OX1 3QR, UK*
[2] *College of Chemistry and Molecular Sciences, Wuhan University, Wuhan 430072, P. R. China.*

*Correspondence to: edman.tsang@chem.ox.ac.uk

With the introduction of Ga^{3+} into Cu/ZnO catalyst precursors, a series of catalysts have been prepared using a simple co-precipitation method and tested as catalysts for the synthesis of methanol from CO_2 hydrogenation. It is found that the presence of a small amount of Ga^{3+} can facilitate thermal deep reduction of ZnO support to Zn atoms under hydrogen prior to catalysis hence a highly active CuZn bimetallic nanoparticle offering catalytic sites is generated. The effect of Ga^{3+} incorporation is attributed to the formation of Ga-containing spinel, $ZnGa_2O_4$ structure, which creates electronic heterojunction with excess ZnO phase to account for the facilitated reduction of Zn^{2+} to Zn^0 to form CuZn when in contact with Cu nanoparticle. A correlation between Zn^0 concentration in the CuZn alloy nanoparticle to the catalytic performance can thus be clearly demonstrated, which shows CO_2 conversion and methanol selectivity can be significantly improved by increasing the Zn^0 content in these hetero-junctioned catalysts.

Introduction

Due to increasing in fossil fuels combustion by the increasing population and human activities, the concentration of carbon dioxide, CO_2, in the atmosphere is rising year by year, which causes a significant global warming. The present attempts to make endeavors to reduce the CO_2 emission, and various technologies for CO_2 capture and transformation are being paid intensive investigation. It has been recently demonstrated that by utilizing solar energy, wind power, hydropower and biomass, renewable hydrogen gas can be produced at large scale[1, 2]. Therefore, the recycling of 'waste' CO_2 through its hydrogenation to high-energy-content fuels such as alcohols or hydrocarbons appears to be a very attractive approach[3]. Particularly, the CO_2 hydrogenation to methanol is becoming a potentially strategic important process due to the positions of methanol as both key chemical platform and clean liquefied fuel. For sustainable development of our society, the feasibility and advantages of the methanol-based economy have recently been advocated by Olah et al [4].

Cu/ZnO based catalysts are well known for methanol synthesis from CO/H_2. Recent research has reported that these catalysts also show superior activity in CO_2 hydrogenation. Cu is usually regarded as the active site but the role of ZnO support is still in debate despite the fact that numerous investigations have been carried out over the past few decades[5-12]. Recently, with the rapid development of advanced characterization techniques, it is shown that a very small amount of Zn atoms is reduced from ZnO and decorate on Cu nanoparticle at the interface, which results a subtle change in the Cu electronic structure[13-15]. Consequently, the high activity is assigned to the formation of this CuZn alloy in contact region[16]. It is however, the mechanism for the deep reduction of support metal ions to corresponding metal atoms is still obscure. On the other hand, it is reported the incorporation of different additives, such as Al_2O_3, ZrO_2, SiO_2 and Ga_2O_3 can further improve the activity, stability and thermal resistance compared with the unmodified Cu/ZnO[16-21]. Recently, using atom probe tomography technique, small, active but stable Cu containing crystallites (~0.5-2 nm) were identified in the working catalyst prepared from Ga^{3+} promoted Cu/ZnO[22-24]. The formation of $ZnGa_2O_4$ spinel structure was believed to play a significant role in the generation of the extremely small Cu clusters under methanol synthesis conditions. However, the promotion mechanism of Ga^{3+} and the nature of active site for the CO_2 hydrogenation are still not yet clear due to some complex solid-solid interaction(s).

On the other hand, semi-conductor materials such like ZnO and $ZnGa_2O_4$ usually play a critical role in catalysis reactions since many working catalysts involve the use of semi-conductor component(s), particularly in the form of metal oxide(s) as support. The catalytic properties of semi-conductor are strongly related with its band structure which can be well-tuned by several methods, doping, hetero-junction, hybridization, morphology control, etc [25,26]. Introducing another semi-conductor modifier to establishing a hetero-junction with a specific energy level alignment is one of the simplest methods for structure tuning, due to a wide range of choices of modifiers and well-acquired skills for their syntheses. There are at least three types of hetero-junctions especially, type II, where the band gaps of two semi-conductors are similar but not at the same band energy positions (as staggered bands) is found to be important in catalysis[27-30]. As to this type II heterojunction, the electrons and holes are spatially separated across the interface during excitation and are localized on different sides of the hetero-interface. Thus, polarization of two carriers over the two semiconductor materials at the interface is taken place. This allows more involvements of these carriers in catalysis processes before their recombination. As a result, some novel properties are usually observed in type II hetero-junction compared with other junctions.

$ZnGa_2O_4$ is a well-known photocatalyst component with wide proposed applications in water splitting and pollutant removal, etc[31]. The integration of ZnO and $ZnGa_2O_4$ forming type II heterojunction was also reported to show enhanced photocatalytic activity compared to the individual components. The enhancement was mainly attributed into the separation of holes and electrons across the interface upon light excitation[31-33], however, the application of this type II heterojunction in thermal catalysis reaction like the present methanol synthesis reaction from CO_2 hydrogenation has not been reported. In this work, it is demonstrated the preparation of a Cu/$ZnGa_2O_4$-ZnO mixture by the introduction of Ga^{3+} into Cu/ZnO. It is shown that Ga^{3+} can readily react with ZnO to form $ZnGa_2O_4$ spinel structure, which thus forms $ZnGa_2O_4$-ZnO heterojunction with excess ZnO where Cu nanoparticles are dispersed upon. With the presence of Ga^{3+} in form of heterojunction, the thermal reduction of ZnO to Zn atom is significantly facilitated. As a result, small CuZn bimetallic nanoparticles are thus generated on the surface of these mixed support phases during reaction. Importantly, the concentration of Zn^0 in the bimetallic phase can be tunable by controlling the amount of Ga^{3+} used in the synthesis. It is also demonstrated that Cu based catalyst with Zn enrichment through the use of heterojunction shows a pronounced enhancement in methanol synthesis from CO_2 hydrogenation reaction.

Methods

Synthesis of Ga^{3+} modified Cu/ZnO catalysts

Ga^{3+} modified Cu/ZnO catalysts were synthesized using a pH-controlled co-precipitation method. The metal precursors were hydrated metal nitrate salts: $Cu(NO_3)_2 \cdot 3H_2O$ (Aldrich), $Zn(NO_3)_2 \cdot 6H_2O$ (Aldrich), and $Ga(NO_3)_3 \cdot 9H_2O$ (Aldrich). For a typical preparation the metal nitrates [3.77g $Cu(NO_3)_2 \cdot 3H_2O$; 5.53g $Zn(NO_3)_2 \cdot 6H_2O$; 0.75g $Ga(NO_3)_3 \cdot 9H_2O$] were dissolved completely in 100 mL deionized water. A Na_2CO_3 aqueous solution was prepared by dissolving 3.50 g of Na_2CO_3 in 100 mL of DI water. The solutions were added simultaneously into a plastic reactor containing 250 mL of preheated DI water. A delivery pump with two 50 mL syringes was used to inject the precursor metal nitrate solution at a constant rate of 0.42 mL/min in an automatic and reproducible manner. An HPLC pump was used to deliver the Na_2CO_3 solution at a rate of 0.35-0.70 mL min^{-1}. The mixture was stirred at 1,000 rpm, with pH of the precipitating solution carefully maintained at 6.5. The precipitation process took place at around 80 °C. The pH of the liquid was measured using a temperature-dependent pH meter and was controlled at pH 6.5, with an error range of ±0.1. Once the addition of the precursor metal nitrate solution was completed, the first aging was carried out under atmospheric conditions to let the pH value to become stable. After 30 mins, the pH was measured again to ensure that the target pH had been reached before putting the lid onto the reactor. The resulting precipitate was continued to the second aging process in solution at 100 °C for 15 h. After aging, the precipitate was extracted by centrifugation at 5,000 rpm. The centrifuged precipitate was washed with DI water five times at 5,000 rpm to remove the residual Na^+ ions. The resulting wet solid was dried in air at 80 °C overnight and then calcined in static air, at a ramp of 5 °C/min up to desired temperature (330°C, otherwise indicated) for 3 h to produce the final catalyst. The catalysts were labelled as CZ (contains no Ga) and CZG-xGa (x indicates the mole % of Ga). The detailed information of the CZ and CZG-xGa catalysts are listed in table 1.

Table 1 Chemical compositions and calcination temperatures of the catalysts used in this study.

Sample	Cu:Zn:Ga (mole %)	Calcination Temperature
CZ	43:57:0	330 °C
CZG-0.5Ga	43:56.5:0.5	330 °C
CZG-5Ga	43:52:5	280 °C
		330 °C
		380 °C
		450 °C
		500 °C
CZG-20Ga	43:37:20	330 °C
CZG-38Ga	43:19:38	330 °C

Catalytic test in CO_2 hydrogenation reaction

Catalyst testing for hydrogenation of CO_2 to produce methanol was carried out in a tubular fixed bed reactor (12.7 mm outside diameter) by placing 0.1 g catalyst sandwiched with glass-wool plugs. Before each test, the catalyst was pre-reduced at 250 °C for 2 h under the H_2 flow of 20 stp mL min^{-1} (stp = standard temperature and pressure; P = 101.3 kPa, T = 298 K). The catalyst bed was then cooled to room temperature. CO_2/H_2 reaction mixture without other gas diluent with molar ratio of 1/2.8 was fed at a rate of 30 stp mL min^{-1} through the catalyst bed, and the system pressure was held at 4.5MPa with the aid of a back-pressure regulator. The reaction temperature was set to 210 °C, 230 °C, 240 °C and 250 °C. The

products were analysed by a gas chromatograph equipped with calibrated thermal conductivity detector (TCD) and flame ionization detector (FID).

Powdered x-ray diffraction (PXRD)

The X-ray diffraction (XRD) profile was collected by a Philips PW-1729 diffractometer with Bragg-Brentano focusing geometry using Cu Kα radiation (lambda= 1.5418 Å) from a generator operating at 40 kV and 40 mA. Table 1 shows the Phase symbol, chemical formula and PDF number which are used in this work.

Table 2, Phase symbol, chemical formula and PDF number which are used in this work.

Phase symbol	Formula	PDF#
A: aurichalcite	$(Cu,Zn)_5(CO_3)_2(OH)_{16}$	82-1253
Z: zincite	ZnO	36-1451
T: tenorite	CuO	05-0661
S: Spinel structure	$ZnGa_2O_4$	86-0415
	$CuGa_2O_4$	44-0183
#: Aluminum	Al	85-1327

X-ray photoelectron spectroscopy (XPS)

After reduction at 250 ^oC, samples were carefully transferred in a glove bag filled with nitrogen to prevent the air exposure and analyzed by XPS. The XPS was performed using a Quantum 2000 Scanning ESCA Microprob instrument (Physical Electronics) equipped with an Al Kα X-ray radiation source (hv = 1486.6 eV). A flood gun with variable electron voltage (from 6 eV to 8 eV) was used for charge compensation. The raw data were corrected for substrate charging with the BE of the C peak (284.5 eV), as reference to the XPS handbook. The measured spectra were fitted using a least-square procedure to a product of Gaussian–Lorentzian functions after removing the background noise. The concentration of each element was calculated from the area of the corresponding peak and calibrated with the sensitivity factor of Wagner.

High-sensitivity low-energy ion scattering (HS-LEIS)

HS-LEIS measurements were carried out on an IonTOF Qtac100 low-energy ion scattering analyzer. Ne^+ ions with a kinetic energy of 5 keV were applied at a low ion flux equal to 445 pA cm^{-2}. The surface composition was obtained from the area of the corresponding peak and calibrated with the sensitivity factors.

Extended X-ray absorption fine structure (EXAFS)

After reduction at 250 ^oC, samples were carefully transferred into capillary tubes (quartz NMR tubes) in a nitrogen glove box. The reduced samples were sandwiched between silica wool to fix the samples in the middle of the capillary tubes, and then the capillary tubes were sealed and stored in a glove box until the EXAFS experiments. Local structures surrounding Cu atoms were probed by using EXAFS technique at beamline BL07A of Taiwan Light Source at National Synchrotron Radiation Research Center (NSRRC) in Taiwan. A Si(111)

Double Crystal Monochromator (DCM) was used to scan the photon energy. The energy resolution ($\Delta E/E$) for the incident X-ray photons was estimated to be 2×10^{-4}. Conventional transmission mode was adopted for Cu K-edge EXAFS measurements. To ascertain the reproducibility of the experimental data, at least two scan sets were collected and compared for each sample. The EXAFS data analysis was performed using IFEFFIT 1 with Horae packages 2 (Athena and Artemes). The spectra were calibrated with Cu foils as a reference to avoid energy shifts of the samples. And the amplitude parameter was obtained from EXAFS data analysis of the foil, which was used as a fixed input parameter in the data fitting to allow the refinement in the coordination number of the absorption element. In this work, the first shell data analyses under the assumption of single scattering were performed with the errors estimated by R-factor.

Field emission transmission electron microscopy (FE-STEM)

Field emission TEM/STEM (FEI Technai F20S-TWIN) was conducted at Johnson Matthey, plc with the help from Dr Winson Kuo using EDAX Si(Li) LN2 EDS detector with SUTW (super ultra-thin window) of active area of 30 mm^2 at the energy resolution of 135eV measured at Mn K alpha.

Temperature programmed and reduction (TPR)

Temperature-programmed reduction (TPR) measurements were obtained using a ThermoQuest TPRO 110 instrument. Inside the TPR quartz tube, 0.026 g of the calcined catalyst sample was sandwiched between two layers of glass wool with a thermocouple placed in contact with the sample. The TPR tube was then inserted into the instrument for a helium pretreatment. The helium gas pretreatment (He running through the TPR tube at 10 mL min^{-1} at a temperature ramp of 10 °C min^{-1} from 40 to 150 °C, then held for 5 min before cooling) cleaned the catalyst surface by removing any absorbed ambient gas molecules. After the pretreatment, a reduction treatment (5% H_2 in Argon flowing through the TPR tube at 20 mL min^{-1} at a temperature ramp of 10 °C min^{-1} from 40 to 330 °C, then held at 330 °C for 30 min before cooling to room temperature) was carried out to reduce the Cu^{2+} within the sample. Cu(II)O was reduced to Cu^0 by the flow of hydrogen gas in the reduction treatment. The consumption of hydrogen gas changed the conductivity of the gas stream; hence, the change in conductivity was measured and calibrated as a function of both temperature and time to produce the TPR profile.

Chemisorption

The reduction treatment of Cu^{2+} to Cu^0 in the catalyst sample (1st TPR) was followed by N_2O chemisorption at room temperature to determine the average size of copper metal particle. Treatment with 5% N_2O/Ar at 20 mL min^{-1} for 40 min was carried out to re-oxidize only the Cu surface via dissociative chemisorption. To remove remaining adsorbed N_2O, another He pre-treatment (He flowing at 10min^{-1} for 10 min at room temperature) was carried out. This was followed by a second reduction treatment (2nd TPR: 5% H_2 in Argon at 20 ml min^{-1} at a temperature ramp of 10 ^oC min^{-1} from 40 ^oC up to 330 ^oC). By analysing data from the first and second TPR, it was possible to determine the Cu surface area of the catalyst sample by pre-calibrating the TPR with a Cu(II)O standard of known Cu content. Standard samples of Cu(II)O: 0.005, 0.0010 and 0.0015 g (Aldrich) were used to perform the TPR and the number of moles of hydrogen consumed was calculated.

Results and discussion

Catalyst characterisation

With the introduction of Ga^{3+} into Cu/ZnO catalyst, a series of catalysts have been prepared using a simple co-precipitation method with carefully control of precursor injection rate, pH value and precipitation temperature. Fig. 1 shows the TPR results of the CZ and CZG samples. It can be noticed that the reduction of CuO to Cu occurred at lower temperature when the sample was doped with Ga^{3+}, which indicates the facilitation of the reduction when Ga was incorporated. In addition, the presence of TPR shoulder peak for the sample with Ga^{3+} content indicates the reduction of Cu^{+} can be detected. According to our previous report[22], it has been proposed that Ga incorporation into Cu/ZnO can lead to the formation of a cubic spinel phase containing interstitial Cu^{+} ions on a defective $ZnGa_2O_4$ surface, which can produce a high population of extremely small copper clusters upon their further reduction for effective catalysis. The physical characterizations of selected CZ and CZG catalysts show that Ga-containing sample (CZG-5Ga, 84.6 m^2g^{-1}) gives higher surface area per gram of catalyst than the unmodified Cu/ZnO sample (CZ, 58.4 m^2g^{-1}). The Cu surface area per gram of catalyst (SA_{Cu}) can also be found to follow the order: CZG-5Ga (63.2 m^2g^{-1}) > CZG-20Ga (53.2 m^2g^{-1}) > CZ (43.0 m^2g^{-1}), suggesting the addition of Ga into Cu/ZnO system can improve the dispersion of Cu due to the presence of Ga-containing cubic spinel phase which helps the formation of small Cu clusters. This result is in agreement with the findings by Schumann et al., who have found that Ga dopant could act as a structure promoter, which resulted high surface area for the Cu catalysts and showed promoted performance in the methanol synthesis condition[34]. In current study, with the addition of Ga^{3+}, the Cu/ZnO catalysts also show enhanced Cu dispersion, which may lead to better performance for those Ga-containing samples in CO_2 hydrogenation to produce methanol.

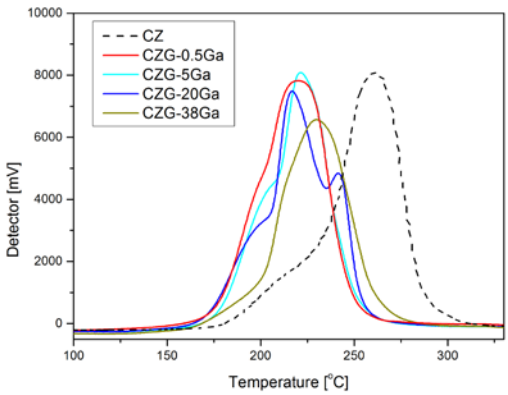

Fig. 1, TPR profiles of calcined CZ and CZG catalysts with different chemical compositions[22].

From the XRD patterns of the calcined sample without the addition of Ga (Fig. 2, CZ), phases of CuO, ZnO, are clearly identified (Table 2). With the progressive Ga addition, a spinel phase of MGa_2O_4 (M = Zn, Cu) was emerged in excess ZnO when Ga was over 0.5% and then dominated the crystallite phases when Ga concentration was higher than 20% (Fig. 2a). The MGa_2O_4 (M = Zn, Cu) spinel phase observed in our calcined catalysts is a well-known semiconductor phase[31]. The integration of ZnO and MGa_2O_4 spinel forming type II electronic heterojunction was also reported to improve the charge separation and enhance catalytic activity compared to the individual components[32,33]. Based on such heterojunction approach, it has been reported that the thermally activated reduction of the refractory metal oxide support could be strongly promoted, which facilitates the formation of bimetallic catalysts with enhanced catalytic performance[30]. Therefore, with the great potentialities of

type II heterojunction effects in our Ga-containing samples, it is logical to anticipate the reduction of ZnO can be facilitated with the help of the MGa_2O_4 and ZnO interfaces, which may facilitate the production of CuZn bimetallic catalyst and alter the catalytic performance of the Cu/ZnO catalysts. Considering CZG-5Ga sample had ZnO and MGa_2O_4 as the most prevalent phases than that in other samples, CZG-5Ga was selected to calcine under different temperatures to see the influences of the calcination conditions. As can be seen in Fig. 2b that CZG-5Ga is initially in form of $(Cu,Zn)_5(CO_3)_2(OH)_{16}$ phase with high dispersion of Ga (Table 2). With the increasing of calcination temperature, MGa_2O_4 could be observed at 330 ^oC, but this phase decomposed into ZnO and CuO phases along with a small amount of Ga_2O_3 (not detected in XRD) as the temperature further raising. From our XRD result, the co-existence of ZnO and the spinel phase can be clearly observed in some CZG samples. Moreover, the relative amounts of these two phases will vary with the synthesis conditions, suggesting that some experimental variables could influence their interfaces and characteristics.

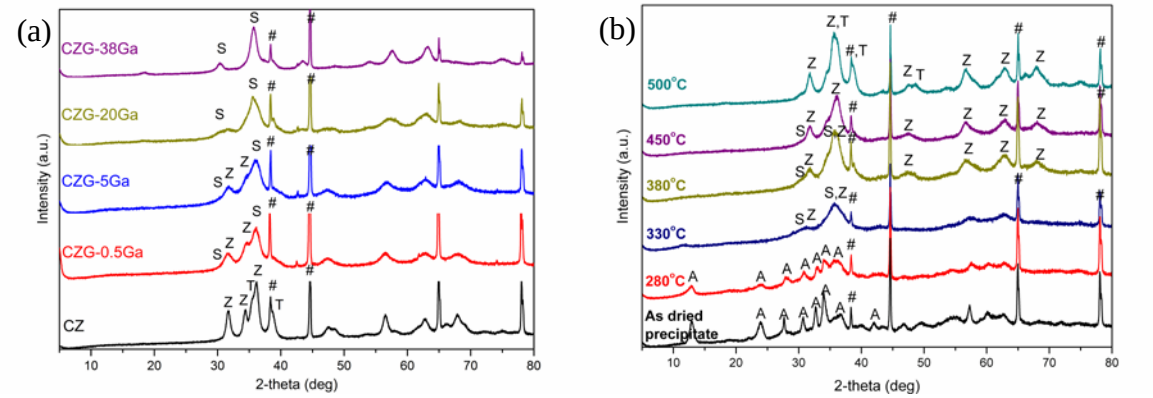

Fig. 2, XRD profiles of calcined CZG catalyst with various (a) chemical compositions; (b) calcination temperatures.

It is clear that two semiconductor solid phases, namely ZnO and spinel structure (MGa_2O_4) can be co-existence under our preparation. In order to reflect the quantity of the ZnO-MGa_2O_4 interfaces, electron energy loss spectroscopy (EELS)-TEM was employed. The EELS elemental mappings for Cu, Zn, Ga and O in the CZG catalysts with varied calcination temperatures are shown in Fig. 3 (left). The brighter area indicates the relatively higher pixel density of a particular element. In order to characterize the interface of the two phases, ZnO and Ga-containing phases (MGa_2O_4), differentiation of the EELS digitalized signal ratios of Zn ($Zn_{L2,3}$ -1020 eV) to Ga ($Ga_{L2,3}$-1115 eV) scanning along a certain region for the samples are displayed in Fig. 3 (right). There are stable flat plateau regions with sharp peaks occasionally observed. For example, the peaks are caused by the drop in Ga concentration from Ga-containing phase to ZnO rich phase. The regions with higher peak frequency within the scan range represent a larger quantity of ZnO-MGa_2O_4 interfaces along the scanned area. From the result, the 330 ^oC sample gives more peaks than all the other samples indicating the 330 ^oC sample gives the largest amount of interfaces between ZnO and the Ga-containing spinel phase. From the results of XRD and EELS-TEM elements mapping, it is concluded that the amount of ZnO-MGa_2O_4 interface can be optimized at 330 ^oC calcined GZG-5Ga sample from the variation of chemical composition and calcination temperature.

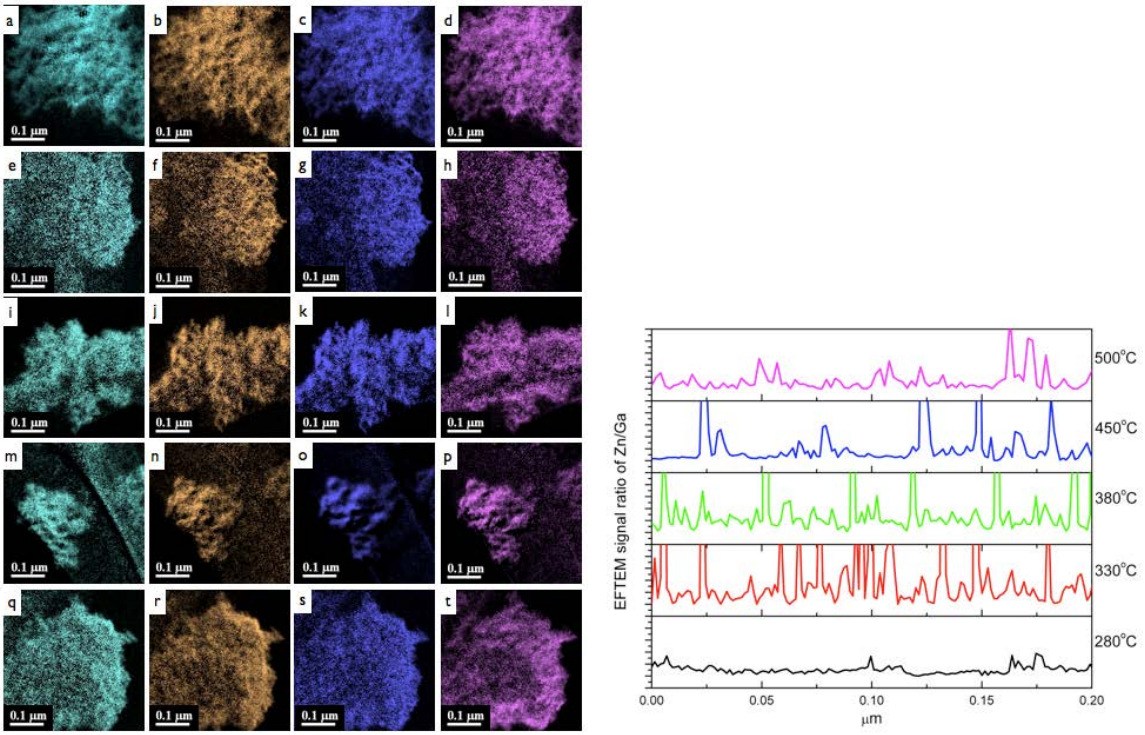

Fig. 3, (a) Left: EELS-TEM mappings of Cu (a,e,I,m,q), Zn (b,f,j,n,r), Ga (c,g,k,o,s) and O (d,h,i,p,t) for sample 280ºC (a,b,c,d), 330ºC (e,f,g,h), 380ºC (i,j,k,l), 450ºC (m,n,o,p) and 500ºC (q,r,s,t); (b) Right: Differential EELS-TEM digital signal ratios of Zn:Ga along a scanning region for 280ºC, 330ºC, 380ºC ,450ºC and 500ºC samples.

From CZ to CZG-5Ga, with the addition of a small quantity of Ga, the energy levels alignment in the catalyst is transformed from type I (CuO-ZnO) heterojunction to type II (MGa_2O_4-ZnO), as shown in Scheme 1 according to their reported bulk energy levels[32,33]. In the CuO-ZnO system, the carriers would thus be confined on the surface of CuO upon thermal excitation. After adding Ga^{3+}, with the formation of the MGa_2O_4 spinel structure, the thermal excited electrons and holes, although in very small quantities, can be separated across the heterojunction interfaces (holes on MGa_2O_4 and electrons on ZnO)[32,33]. Due to this spatial separation of excitons, the lifetime of the carriers in GZG-5Ga is expected to increase.

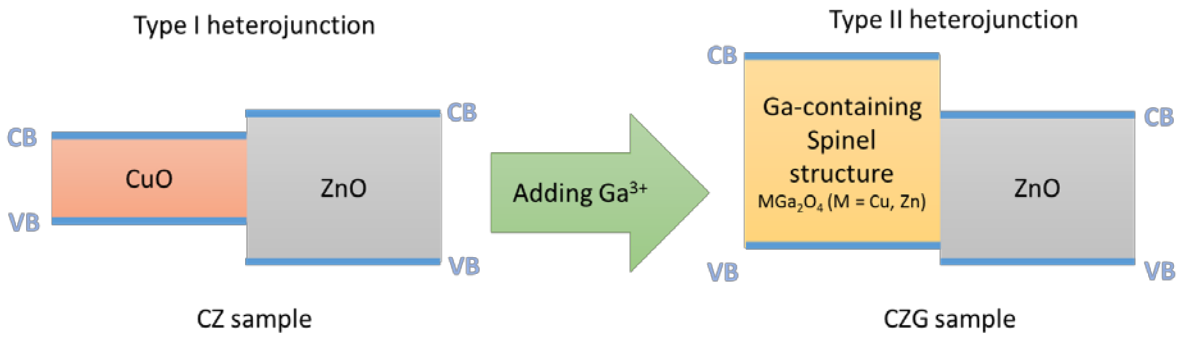

Scheme 1. Energy levels alignments in the CZ and CZG samples

In order to confirm the enhanced lifetime for the charge carriers in this system, time-resolved photoluminescence (TRPL) measurement was conducted with 300 nm light excitation source

for the CZ and CZG-5Ga samples (both were calcined at 330 ^{o}C) to further investigate the influence of the type II heterojunction. It is noted that light excitation is more efficient than thermal means hence it is easier to follow the TRPL at higher charge carrier concentration. Fig. 4 shows the experimental decay profiles, derived from the integration of the TRPL. The curves are fitted using multi-exponential function to obtain the time constants (τi) and associated fractional contributions (ai%). As seen from Table 3, the fractions of the long-lived components (a2, a3) in CZG-5Ga sample are indeed higher than that in the CZ sample, which implies the increased fraction of non-instant recombination of the carriers in CZG-5Ga by the formation of type II heterojunction. Moreover, the lifetimes of these long-lived components in CZG-5Ga sample (21, 150 ns) are significantly longer than those of CZ sample (20, 130 ns). Therefore, from the TRPL result, it is clear that the type II heterojunction of ZnO-MGa_2O_4 in CZG-5Ga sample enhances the spatial separation of excited electrons and holes across the interface which reduces the rapid instant recombination and prolongs their lifetime.

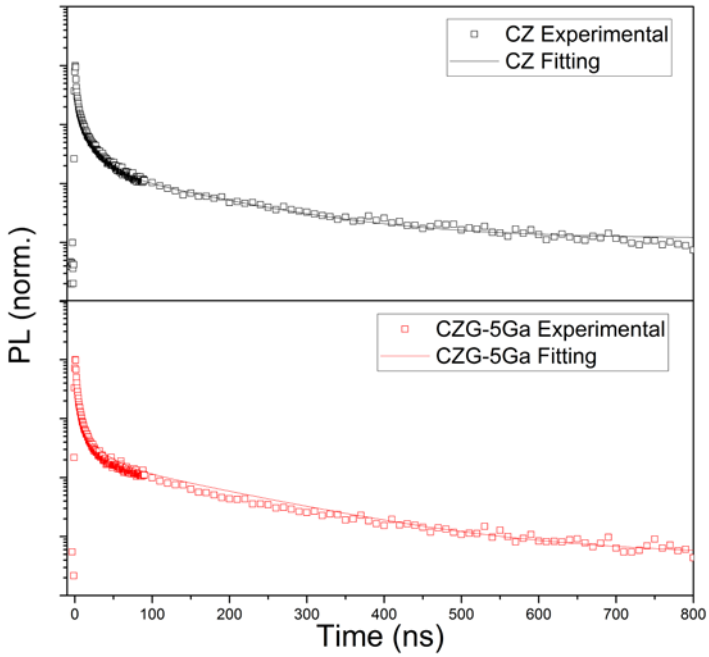

Fig. 4, experimental and fitted kinetic decay profiles obtained from integrated intensity of the time-resolved emission spectra of samples.

Table 3 Exponential decay components of fractional emission amplitudes of CZ and CZG-5Ga samples

Sample	τ1 (ns)	a1 (%)	τ2 (ns)	a2 (%)	τ3 (ns)	a3 (%)
CZ	5	85.9	20	12.5	130	1.6
CZG-5Ga	3	80.4	21	14.5	150	5.1

As a typical semi-conductor oxide, some thermal- or photo- excited electrons could momentarily overcome the forbidden band gap and occupy the higher energy conduction band which is primarily composed of empty bands of cations. The corresponding 'holes' will take residence in the lower energy valence band that is constituted mainly by occupied p-bands of oxygen ions. Thus, the term 'hole' in semiconductor oxide can be appreciated chemically as *activated oxygen species* with lower formal charge (neutral or singularly charged oxygen) than lattice oxygen ions. However, majority of the excited electrons and holes (excitons) will recombine rapidly in the single phase semi-conductor oxide support with short lifetime as reflected by the TRPL data. On the other hand, with the establishment of type II heterojunction of ZnO-MGa_2O_4, particularly in CZG-5Ga (calcined at 330 ^oC), more activated oxygen species and holes are accumulated in MGa_2O_4 and ZnO region, respectively, as indicated by the increased fractions of long-lived components in TRPL. In the H_2 pre-treatment process, these activated oxygen species (holes) could then react with spilled H in a close proximity to Cu metal nanoparticle to form water as their long lifetime allows the occurrence of this chemical reaction. Thus, corresponding electrons in ZnO region will reduce Zn^{2+} from the support mixture to Zn atoms.

The XPS spectra were collected and analysed. We did not see any evidence on the existence of metallic Ga (mainly Ga^{3+} was detected). It is noted that Nørskov and co-workers have recently shown Ni-Ga alloy catalysts are also effective for methanol synthesis from CO_2/H_2 [35]. On the other hand, there appeared to have reduction of ZnO to metallic Zn atoms. The XPS results of the reduced samples with various amount of Ga content and calcination temperature are revealed in Fig. 5. It clearly shows that Zn 2p curves can be deconvoluted into two peaks of Zn^{2+} (1023 eV) and Zn^0 (1021 eV). According to the peak area of signals, the Zn^0/Cu ratios were calculated and presented in Fig. 5b and 5c. Clearly, the Zn^0/Cu values reach the peaks at GZG-5Ga calcined 330 ^oC sample, indicating the highest concentration of Zn^0 present in this sample, which is resulted from the highest amount of ZnO-MGa_2O_4 type II heterojunction interfaces as characterized by XRD and TRPL. On the other hand, the lowest ratio of Zn^0/Cu in CZG-38Ga was attributed to the single phase of spinel structure in the support as indicated by the XRD result. In order to obtain the accurate composition information of the topmost surface of the catalysts, high sensitivity low-energy ion scattering (HS-LEIS) measurements using Ne^+ were also applied. Fig. 6 with an inserted table shows the HS-LEIS result of CZ sample and CZG-5Ga sample. The XPS result for each sample is presented as a comparison. As seen from Fig. 6, CZG-5Ga contains higher concentration of Zn species on the outmost surface compared to the CZ sample, which further confirms the surface enrichment of Zn by the promotion of type II heterojunction. With the combined results of XPS, HS-LEIS with XRD and EF-TEM mapping, it is clearly established that the addition of an appropriate amount of Ga^{3+} promotes the formation of ZnO-MGa_2O_4 heterojunction interfaces which play a key role in facilitating the reduction of ZnO to Zn^0, as shown in Fig.7. Therefore, the optimal Zn^0 reduction point is located at the catalyst mixture with most prominent heterojunction effect (5% Ga^{3+} and 330 ^oC calcination temperature).

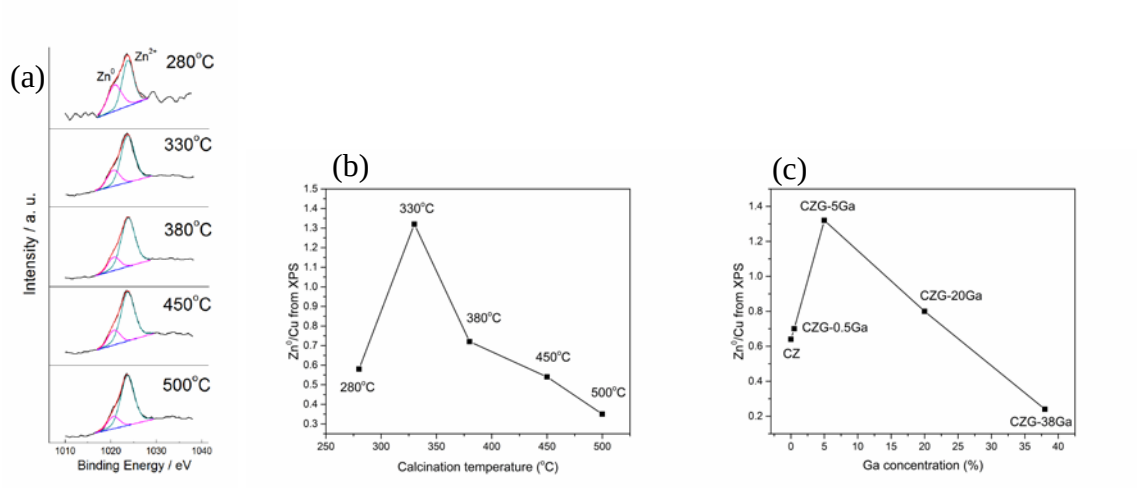

Fig. 5, (a) XPS Zn 2p peaks of the CZG-5Ga with 280 ºC, 330 ºC, 380 ºC, 450 ºC and 500 ºC calcination temperature, and the plots of Zn^0/Cu ratios derived from XPS analysis to various (b) calcination temperature and (c) Ga concentration.

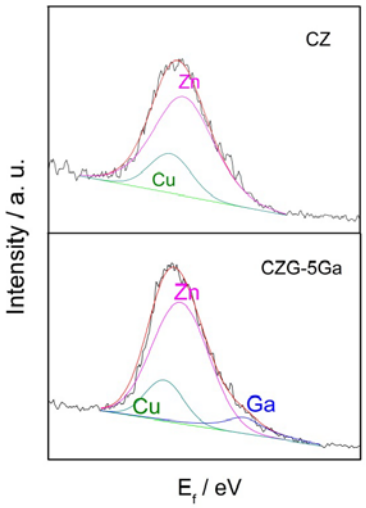

Catalyst	Method	Zn/Cu atomic ratio
CZ	HS-LEIS	3.72
	XPS	3.46
CZG-5Ga	HS-LEIS	4.42
	XPS	4.14

Fig. 6, HS-LEIS (High Sensitivity Low-Energy Ion Scattering**) at 5 keV Ne^+ and the list of Zn/Cu and Zn/Ga ratios from XPS and HS-LEIS for CZ and CZG-5Ga samples.**

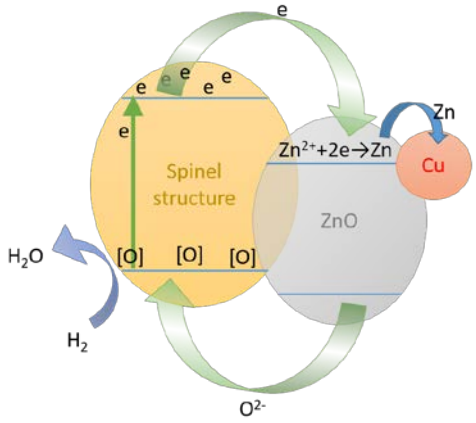

Fig. 7, The electron flow circle in the reduction process of ZnO to Zn catalyzed by $ZnGa_2O_4$

Given the intimate interface of Zn-containing phase and Cu-containing phase in the materials, the produced Zn^0 will decorate or react with the Cu nanoparticle to form bimetallic nanoparticles. X-ray absorption spectroscopy (XAS) measurements were carried out at the Cu K-edge for the reduced CZ and CZG-5Ga samples to reveal the interaction between Cu and Zn atoms. The first shell data analysis has been performed with the consideration of the systematic errors in the coordination number of the absorbing atom and the inter distances between the absorbing atom and neighboring atoms. To perform the EXAFS fitting, Cu metal with a face centered cubic (*fcc*) structure was taken as the primary model to generate the scattering path of Cu-Cu (2.56Å). It was found that the spectra of the CZG-5Ga sample could not be modeled using only scattering parameters from metallic Cu. Therefore, CuZn alloy structure with a body centered cubic (*bcc*) structure was then taken to generate the scattering paths of Cu-Zn (2.56Å) and Cu-Cu (2.99Å) for the CZG-5Ga sample. Notice that the longer distance of Cu-Cu (2.99Å) in *bcc* CuZn model is distinctive from the shorter Cu-Cu (2.56Å) of *fcc* metallic Cu model and *fcc* Cu-Zn (2.56Å) of CuZn model. The experimental data for the reduced CZ and CZG-5Ga samples were recorded and satisfactory R fittings were achieved, as shown in Fig. 8 and Table 4. As can be seen in Table 4, all R-factors are below 0.8% with the coordination number derived from 2.56Å scattering path around 8.6 to 8.8. Interestingly, the coordination number of Cu-Cu bond (2.99Å) derived from CuZn alloy is 1.7 in the CZG-5Ga sample, suggesting CuZn nano alloys were present. However, for the CZ sample, no Cu-Cu 2.99Å bond was observed which indicates no body centered CuZn alloy formed after the reduction procedure.

Table 4 Cu K-edge EXAFS result for CZG-5Ga and CZ samples

Catalyst	enot	CN (*bcc* Cu-Zn & *fcc* Cu-Cu)	D-W factor (*bcc* Cu-Zn & *fcc* Cu-Cu)	Bond length (Å) (*bcc* Cu-Zn & *fcc* Cu-Cu)	CN (*bcc* Cu-Cu)	D-W factor (*bcc* Cu-Cu)	Bond length (Å) (*bcc* Cu-Cu)	R-factor
CZG-5Ga	2	8.6(2)	0.010(1)	2.53(1)	1.7(3)	0.012(4)	2.96(2)	0.4%
CZ	3.4	8.8(3)	0.009(1)	2.54(1)				0.8%

(Note: Enot is the energy difference of absorption energy in experimental value and the calculated value; *bcc* Cu-Zn, *fcc* Cu-Cu and *fcc* Cu-Zn all give 2.56 Å according to their models, however, for *bcc* Cu-Zn, a longer Cu-Cu of 2.99Å is particularly noted)

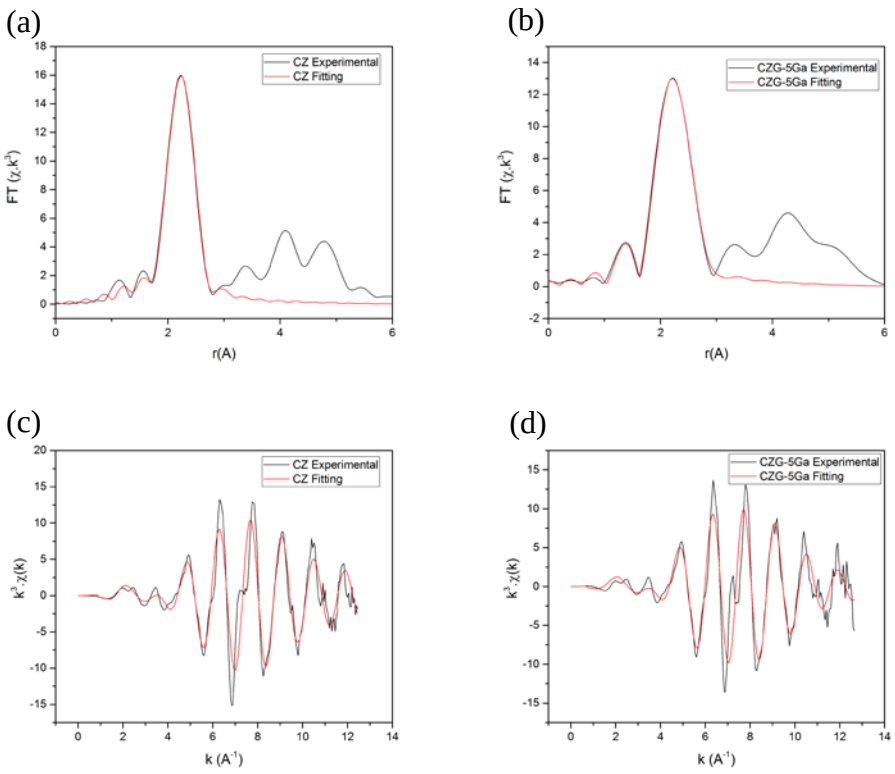

Fig. 8, EXAFS plots of: (a) $k^3.\chi$ phase corrected Fourier transform of experimental and fitted data for CZ; (b) $k^3.\chi$ phase corrected Fourier transform of experimental and fitted data for CZG; (c) $k^3.\chi$ experimental and fitted data for CZ; (d) $k^3.\chi$ experimental and fitted data for CZG.

The identification of *bcc* CuZn alloy is rather challenging due to the similar properties (atomic size, crystallite structure, etc.) in Cu and Zn atoms. By using EXAFS technique, we have determined the presence of body centered CuZn alloy in the reduced CZG-5Ga sample. It is known that in the Cu-Zn system, when the Zn concentration is high enough (>50% in bulk system), the CuZn alloy tends to change the structure from face centered cubic (*fcc*) to body centered cubic (*bcc*)[36]. In our EXAFS result, we have identified the presence of high Zn-containing CuZn structure (*bcc* CuZn), suggesting that with the promotion of heterojunction effect, the reduced Zn^0 is abundant in the vicinity of Cu atoms, which stabilizes the *bcc* CuZn alloy. To further confirm the presence of *bcc* CuZn alloy, the HR-STEM analysis was performed. Fig. 9 shows the HR-STEM images of the reduced CZG-5Ga (Fig. 9a-9c) and CZ (Fig. 9d-9f) samples and the corresponding fast-Fourier Transform (FFT) analyses of the selected areas. As shown in Fig. 9b, the pattern in area 1 is indexed to the *bcc* CuZn alloy whereas that in the area 3 (Fig. 9c) indicates the presence of a *fcc* structure, which could be *fcc* metallic Cu or *fcc* CuZn alloy. On the other hand, no *bcc* CuZn alloy can be found in the reduced CZ sample (see Fig. 9e and 9f), presumably due to the relatively low content of Zn^0 in the reduced catalyst, which is also depicted by XPS and HS-LEIS.

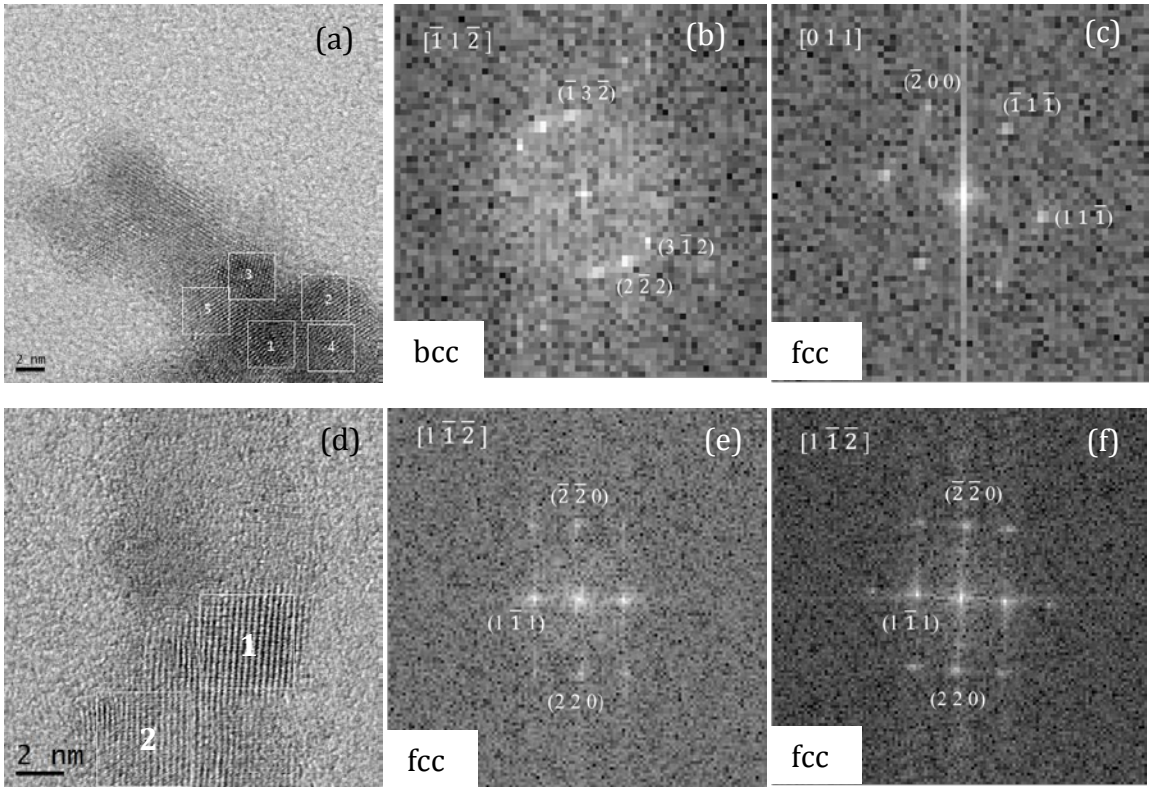

Fig. 9, High-resolution STEM image of the small regions in the reduced CZG-5Ga sample (a) and the fast-Fourier transform (FFT) patterns of area 1 (b) and 3 (c) in (a); with the reduced CZ sample (d) and the fast-Fourier transform (FFT) patterns of area 1 (e) and 2 (f) in (d).

CO_2 hydrogenation

To investigate the influence of Zn^0 concentration, the reaction of CO_2 hydrogenation to synthesize methanol was performed. Fig. 10 shows the methanol yield of the CZ and CZG samples under different reaction temperatures. In general, CZG-5Ga shows better performance than all the other samples. The methanol yield reaches the optimal value at 240 ^oC and drops with further increasing temperature, which suggests the approach of the thermodynamic limit. Therefore, the results obtained at 240 ^oC for the series of CZG samples with various Ga additions were selected and presented in Fig. 11 to compare with each other. Interestingly, both the conversion and methanol selectivity show the same change trend in the order of CZG-38Ga < CZ < CZG-0.5Ga < CZG-20Ga < CZG-5Ga (Fig. 11a). In addition, a strong correlation in Zn^0 concentration to the catalytic performance can be observed: Fig. 11b clearly indicates that activity and selectivity follow closely to the Zn^0/Cu ratio, suggesting the formation of CuZn alloy, promoted by the presence of heterojunction, helps to improve the catalytic performance. CZG-5Ga shows the best conversion (27%) and methanol selectivity (50%) due to its highest Zn^0 content promoted by the pronounced type II heterojunction. From CZ to CZG-5Ga, the methanol yield is raised up to 1.5 times. On the other hand, CZG-38Ga with only pure MGa_2O_4 spinel phase as the support (no heterojunction effect) has the least amount of Zn^0, its concentration of the active species is reduced due to the increasing of non-active Ga species, which results the least activity and selectivity.

By controlling the content of Ga addition, different phase mixture in the catalysts can be obtained. The formulation of the solid phases greatly affects the amount of solid interfaces and the nanostructure of the Cu catalysts, which alter the catalytic performance of CO_2 hydrogenation.

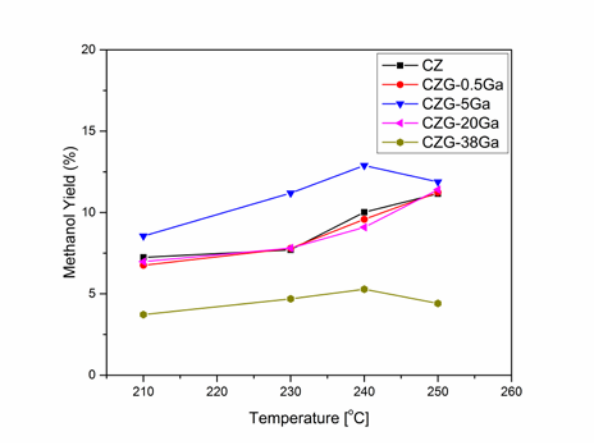

Fig. 10 Methanol yield of CO_2 hydrogenation reaction over CZ and CZG samples prepared with various chemical compositions (all calcined at 330ºC).

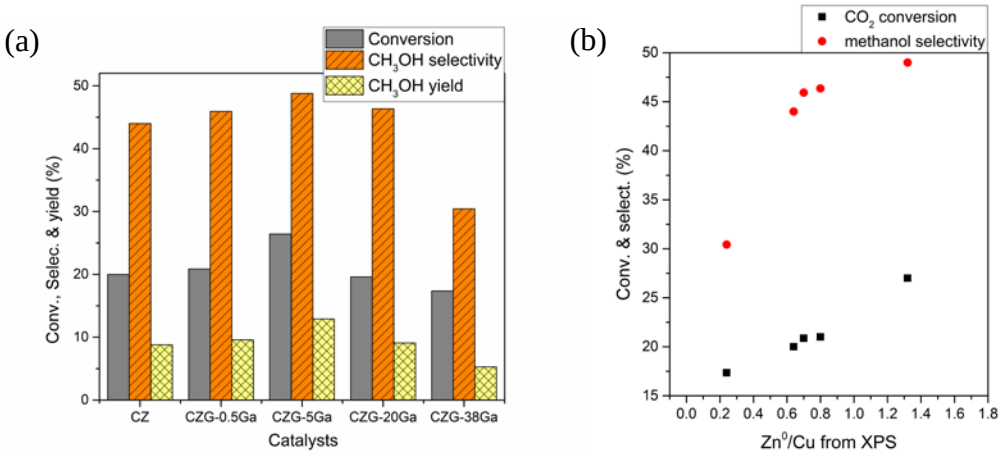

Fig. 11 (a) Catalytic performances of CZ and CZG samples prepared with various chemical compositions (all calcined at 330ºC) under CO_2 hydrogenation reaction condition of 240°C. b) The correlation between Zn^0/Cu obtained from XPS result with CO_2 hydrogenation catalytic performances at 240°C of CZ and CZG samples.

Discussion:

Although it is widely accepted that the presence of ZnO increases the activity of Cu catalysts towards methanol synthesis from extensive experimental works, the nature of material interaction(s) and the 'activate site' are still under debate. As a result, the enhancement of the activity of Cu by ZnO is crudely assigned to so called 'strong metal-support interactions' (SMSI) [37-39] with no specificity in the interaction. There have been a number of proposals to account for this effect, which includes the textural contribution of ZnO to disperse Cu particles[22-24] and the formation of low coordinate Lewis acid Zn sites to assist activation[40].

Similarly, the effect of Ga to promote catalytic performance of Cu/ZnO for methanol synthesis is not yet known despite the fact that Ga dopant is generally well known to promote hydrogenation reactions. Proposed mechanisms include its improvement of Cu dispersion[34], facilitation of Ga_2O_3 to stabilize Cu^0/Cu^+ [41], Lewis acid Zn/Ga sites to assist dihydrogen activation[42,43] and the electronic promotion to Cu[44], etc.

Indeed, according to Schumann et al, they have found a strong electronic effect of Ga in promoting Cu/ZnO catalysts in reversed water gas shift reaction. However, for the methanol synthesis, they attributed the main effect of adding Ga dopant as a structure promoter (increase the surface area and the dispersion of Cu)[34]. Under reaction conditions of 20 bar,

H_2/CO_2 = 3/1, Toyir et al. found 99.5% selectivity can be achieved over their Ga promoted Cu/ZnO catalysts. With taken the reversed water-gas shift (RWGS) equilibrium into account (fine divided Cu metal particle is an excellent catalyst for RWGS) this selectivity appears to be unexpectedly high. This may relate to the difficulties in the actual gas analysis at their very low conversions (2 to 5%). Nevertheless, they attributed the high performance to the presence of Ga_2O_3 particles at the surface of Cu-ZnO-Ga_2O_3/SiO_2, which stabilized Cu^0/Cu^+ catalysis. But, the precise effect of Ga_2O_3 and the mechanism on activity promotion were not specified[41]. Kazansky and co-workers argued that the low coordinated reduced Ga ion, as similar to Zn ion, may provide active Lewis acid sites to assist the activation of hydrogen[42,43]. The recent observation by Martin et al. on unusual conductivity ZnO under the reactions conditions is intriguing, which may suggest a strong electronic promotion to the Cu in the catalyst mixture[44].

In the rich context of the above literature for the Zn/Ga promotion effects on Cu in methanol, we did not discount the structural contribution made by the Ga dopant. In fact, we have showed the enhancement in the dispersion of Cu with Ga promotion. As a result, the textural contribution to Cu/ZnO in the Ga incorporation appears to play a role in the activity promotion. More importantly, Nørskov and Schlögl and co-workers[16] have recently used advanced characterization techniques to demonstrate a very small amount of reduced Zn atoms from ZnO, which decorated on Cu nanoparticle at the interface resulting in a subtle change in Cu electronic structure. They assigned the active sites as Cu steps decorated with Zn atoms by the DFT calculations. From our present catalytic results, we can see a clear correlation of catalytic performance to the concentration of Zn^0 on the surface of Cu due to electronic interactions between catalytic components. Thus, we believe it is timely, to re-emphasise the electronic interactions of Ga promoted Cu/ZnO catalysts for this industrial important reactions. The recent observation by Martin et al. on the ZnO becoming conductive under the reactions conditions is no doubt interesting. They attributed the methanol activity to the electron transfer of this phase to stabilize copper in reduced state. We believe that such observation and proposed mechanism might not necessary contradict to our present observations. It is well accepted that a high degree of reduction of ZnO to Zn (in our case, promoted by the presence of heterojunction) can subtly change the concentration of fundamental species (vacancies and interstitials) in ZnO, which leads to enhanced conductivity and stabilization of Cu by the reduced Zn atoms. Thus, indeed, such transformation of ZnO to conductive phase could support the formation of heterojunction in our case. At present, there might be shortcomings in our study since our samples were not characterized under in-situ or operando conditions due to the unavailability of facilities under our elevated temperature and pressure (250 ^oC, 45 bars) and fouling of the catalyst surface, etc during the catalysis, we aim to perform further characterization under operational conditions in the future.

Conclusions

This study shows the significant influences by the incorporation of Ga^{3+} into Cu/ZnO catalysts. Apart from the structural promotion provided by Ga^{3+} species, our results clearly indicate that the introduction of Ga^{3+} into Cu/ZnO catalyst precursor facilitates the deep reduction of ZnO support to Zn^0 by the establishment of electronic heterojunction of ZnO-MGa_2O_4 (M = Zn or Cu). The reduced Zn^0 when in contact with Cu nanoparticle can form CuZn, which are confirmed by EXAFS and HR-STEM techniques. It is found that the increase of Zn^0 concentration in the catalysts can enhance the catalytic performance of the reaction of methanol synthesis from CO_2 hydrogenation. Both activity and selectivity are dramatically improved after adding an appropriate amount of Ga^{3+} into Cu/ZnO system which results in a pronounced type II heterojunction effect. As stated in the introduction, the

recent paper of Nørskov and Schlögl and their further DFT works clearly suggest that alloying of Zn into the Cu step further increases the adsorption strength of HCO, H_2CO and H_3CO surface intermediates and decrease their barriers to methanol, hence the rate can be dramatically promoted[16]. Thus, the proposed facilitated reduction of ZnO in the presence of Ga^{3+} giving more CuZn can promote higher activity for the methanol synthesis. Overall, this type II heterojunction concept could provide a generic method for tuning thermal reduction behavior of metal oxide support to metallic atoms which consequently influences the properties of overlying metal nanoparticles through the formation of bimetallic phase at the interface. This allows the rational design of catalyst with optimal performance.

Acknowledgements

We wish to thank the finance support from the EPSRC, UK. MMJL kindly acknowledges the receipt of Swire Scholarship for her DPhil study at the University of Oxford, UK. We are indebted to the EELS-TEM characterization by Prof. Heyong He and Dr Renchao Che of Fudan University, China; Dr Wai-Ming Kwok of Hong Kong Polytechnics University for his help on the TRPL; Dr Winson Kuo of Johnson Matthey Technology Centre, UK for the STEM works and Prof. Yun-Liang Soo and Tai-Sing Wu for the access of EXAFS of Taiwan Light Source at National Synchrotron Radiation Research Center (NSRRC).

References

1. Yu, K. M. Curcic, I. Gabriel, J. & Tsang, S. C. E. Recent advances in CO_2 capture and utilization. *ChemSusChem*. **1**, 893-899 (2008).
2. Turner, J. et al. Renewable hydrogen production. *Int. J. Energy Res*. **32**, 379-407 (2008).
3. Song, C. Global challenges and strategies for control, conversion and utilization of CO_2 for sustainable development involving energy, catalysis, adsorption and chemical processing. *Catal. Today*. **115**, 2-32 (2006).
4. Olah, G. A. Beyond Oil and Gas: The Methanol Economy. *Angew. Chem. Int. Ed*. **44**, 2636-2639 (2005)
5. Fujitani, T. Nakamura, J. The chemical modification seen in the Cu/ZnO methanol synthesis catalysts. *Appl. Catal. A*. **191**, 111-129 (2000).
6. Liao, F. Zeng, Z. Eley, C. Lu, Q. Hong, X. & Tsang, S. C. E. Electronic modulation of a copper/zinc oxide catalyst by a heterojunction for selective hydrogenation of carbon dioxide to methanol. *Angew. Chem. Int. Ed*. **51**, 5832-5836 (2012).
7. Zander, S. et al. The role of the oxide component in the development of copper composite catalysts for methanol synthesis. *Angew. Chem. Int. Ed*. **52**, 6536-6540 (2013).
8. Spencer, M.S. The role of zinc oxide in Cu/ZnO catalysts for methanol synthesis and the water-gas shift reaction. *Top. Catal*. **8**, 259-266 (1999).
9. Fujitani, T. & Nakamura, J. The effect of ZnO in methanol synthesis catalysts on Cu dispersion and the specific activity. *Catal. Lett*. **56**, 119-124 (1998).
10. Kanai, Y. et al. Evidence for the migration of ZnO_x in a Cu/ZnO methanol synthesis catalyst. *Catal. Lett*. **27**, 67-78 (1994).
11. Fujita, S. Usui, M. Ito, H. Takezawa, N. Mechanisms of methanol synthesis from carbon dioxide and from carbon monoxide at atmospheric pressure over Cu/ZnO. *J. Catal*. **157**, 403-413 (1995).
12. Choi, Y. Futagami, K. Fujitani, T. Nakamura, J. The role of ZnO in Cu/ZnO methanol synthesis catalysts - morphology effect or active site model? *Appl. Catal. A*. **208**, 163-167 (2001).

13. Hambrock, J. Schröter, M. K. Birkner, A. Wöll, C. & Fischer. R. A. Nano-brass: Bimetallic copper/zinc colloids by a nonaqueous organometallic route using [Cu(OCH(Me)$CH_2NMe_2)_2$] and Et_2Zn as Precursors. *Chem. Mater.* **15**, 4217-4222 (2003).
14. Sanches, S. G. Huertas, F. J. de Avillez, R. R. & Pais da Silva, M. I. Influence of preparation methods and Zr and Y promoters on Cu/ZnO catalysts used for methanol steam reforming. *Int. J. Hydrogen Energy* **37**, 6572-6579 (2012).
15. Derrouiche, S. Lauron-Pernot, H. & Louis. C. Synthesis and treatment parameters for controlling metal particle size and composition in Cu/ZnO materials-first evidence of Cu_3Zn alloy formation. *Chem. Mater.* **24**, 2282-2291 (2012).
16. Behrens, M. et al. The active site of methanol synthesis over Cu/ZnO/Al_2O_3 industrial catalysts. *Science.* **336**, 593-897 (2012).
17. Arena, F. Barbera, K. Italiano, G. Bonura, G. & Spadaro, L. Synthesis, characterization and activity pattern of Cu-ZnO/ZrO_2 catalysts in the hydrogenation of carbon dioxide to methanol. *J. Catal*. **249**, 185-194 (2007).
18. Saito, M. Fujitani, T. Takeuchi, M. & Watanabe, T. Development of copper/zinc oxide-based multicomponent catalysts for methanol synthesis from carbon dioxide and hydrogen. *Appl. Catal. A.* **138**, 311-318 (1996).
19. Kurtz, M. Wilmer, H. Genger, T. Hinrichsen, O. & Muhler, M. Deactivation of supported copper catalysts for methanol synthesis. *Catal. Lett.* **86**, 77-80 (2003).
20. An, X. et al. A Cu/Zn/Al/Zr Fibrous Catalyst that is an Improved CO_2 Hydrogenation to Methanol Catalyst. *Catal. Lett.* **118**, 264-269 (2007).
21. Weigel, J. Koeppel, R. A. Baiker, A. & Wokaun, A. Surface species in CO and CO_2 hydrogenation over copper/zirconia: On the methanol synthesis mechanism. *Langmuir*. **12**, 5319-5329 (1996).
22. Yu, K. M. et al. Non-syngas direct steam reforming of methanol to hydrogen and carbon dioxide at low temperature. *Nat. Commun*. **3**, 1230 (2012).
23. Tong, W. Cheung, K. West, A. Yu, K. M. & Tsang, S. C. E. Direct methanol steam reforming to hydrogen over CuZnGaOx catalyst without CO post-treatment: Mechanistic considerations. *Phys. Chem. Chem. Phys.* **15**, 7240-7248 (2013).
24. Tong, W. West, A. Cheung, K. Yu, K. M. & Tsang, S. C. E. Dramatic effects of gallium promotion to methanol steam reforming Cu-ZnO catalyst for hydrogen production: Formation of 5 A copper clusters from $CuZnGaO_x$. *ACS catal*. **3**, 1231-1244 (2013).
25. Smith, A. M. & Nie, S. Semiconductor nanocrystals: structure, properties, and band gap engineering. *Acc Chem Res*. **43**, 190-200 (2010).
26. Yin, L. & Bando, Y. Semiconductor morphology: Optimizing properties by tuning morphology. *Nat. Mater*. **4**, 883-884 (2005).
27. Chen, C. Y. et al. Spectroscopy and femtosecond dynamics of type-II CdSe/ZnTe core-shell semiconductor synthesized via the CdO precursor. *J. Phys. Chem. B*. **108**, 10687-10691 (2004).
28. Chou, P. T. et al. Spectroscopy and femtosecond dynamics of type-II CdTe/CdSe core-shell quantum dots. *ChemPhysChem*, **7**, 222-228 (2006).
29. Kaniyankandy, S. Rawalekar, S. Verma, S. & Ghosh,H. N. Ultrafast hole transfer in CdSe/ZnTe type II core-shell nanostructure. *J. Phys. Chem. C*. **115**, 1428-1435 (2011).
30. Liao, F. L. et al. A new class of tunable heterojunction by using two support materials for the synthesis of supported bimetallic catalysts. *ChemCatChem.* **7**, 230-235 (2015).
31. Li, Z. et al. Controlled synthesis of $ZnGa_2O_4$ nanorod arrays from hexagonal ZnO microdishes and their photocatalytic activity on the degradation of RhB. *RSC Adv*. **4**, 48590-48595 (2014).

32. Ma, B. Lin, K. Su, W. & Liu, W. One-pot synthesis of ZnO/$ZnGa_2O_4$ heterojunction with X/XY structure for improved photocatalytic activity. *Appl. Surf. Sci.* **317**, 682-687 (2014).
33. Babu, V. J. Vempati, S. Uyar, T. & Ramakrishna, S. Review of one-dimensional and two-dimensional nanostructured materials for hydrogen generation. *Phys. Chem. Chem. Phys.* **17**, 2960-2986 (2015).
34. Schumann, J. Eichelbaum, M. Lunkenbein, T. Thomas, N. Galván, M. C. A. Schlögl, R. & Behrens, M. Promoting strong metal support interaction: doping ZnO for enhanced activity of Cu/ZnO:M (M = Al, Ga, Mg) catalysts. ACS Catal. 5, 3260-3270 (2015).
35. Studt, F. et al. Discovery of a Ni-Ga catalyst for carbon dioxide reduction to methanol. *Nature Chem.* **6**, 320-324 (2014).
36. Ahlers, M. Martensite and equilibrium phases in Cu-Zn and Cu-Zn-Al alloys. *Prog. Mater. Sci*. **30**, 135-186 (1986).
37. Grunwaldt, J. D. Molenbroek, A. M. Topsøe, N. Y. Topsøe, H. & Clausen, B. S. In situ investigations of structural changes in Cu/ZnO catalysts. *J. Catal.* **194**, 452-460 (2000).
38. Naumann d'Alnoncourt, R. Xia, X. Strunk, J. Loffler, E. Hinrichsen, O. & Muhler, M. The influence of strongly reducing conditions on strong metal-support interactions in Cu/ZnO catalysts used for methanol synthesis. *Phys. Chem. Chem. Phys.* **8**, 1525-1538 (2006).
39. Kuld, S. Conradsen, C. Moses, P. G. Chorkendorff, I. & Sehested, J. Quantification of zinc atoms in a surface alloy on copper in an industrial-type methanol synthesis catalyst. *Angew. Chem. Int. Ed.* **53**, 5941-5945 (2014).
40. Fichtl, M. B. Schumann, J. Kasatkin, I. Jacobsen, N. Behrens, M. Schlögl, R. Muhler, M. & Hinrichsen, O. Counting of oxygen defects versus metal surface sites in methanol synthesis catalysts by different probe molecules. *Angew. Chem. Int. Ed.* **53**, 7043-7047 (2014).
41. Toyir, J. Ramírez de la Piscina, P. Fierro J. L. G. & Homs, N. Highly effective conversion of CO_2 to methanol oversupported and promoted copper-based catalysts: influence of support and promoter. *Appl. Catal. B.* **29**, 207-215 (2001).
42. Kazansky, V. B. & Pid'ko, E. A. Diffuse Reflectance IR Spectra of molecular hydrogen and deuterium adsorbed on zinc oxide. *Kinet. Catal.* 43, 567-572 (2002).
43. Kazansky, V. B. Subbotina, I. R. Pronin, A. A. Schlögl, R. & Jentoft, F. C. Unusual infrared spectrum of ethane adsorbed by gallium oxide. *J. Phys. Chem. B.* **110**, 7975-7978 (2006).
44. Martin, O. Mondelli, C. Curulla-Ferré, D. Drouilly, C. Hauert, R. & Pérez-Ramírez, J. zinc-rich copper catalysts promoted by gold for methanol synthesis. *ACS Catal.* **5**, 5607-5616 (2015).